Thin Solid Films, *120* (1984) 81–108
ELECTRONICS AND OPTICS

OPTICAL PROPERTIES OF D.C. REACTIVELY SPUTTERED THIN FILMS

YIN ZHIQIANG* AND G. L. HARDING
School of Physics, University of Sydney, Sydney 2006 (Australia)
(Received December 20, 1983; accepted June 12, 1984)

Deposition parameters, compositions and optical constants n and k have been determined for a range of reactively sputtered composite materials produced in d.c. post cathode magnetron sputtering systems. Optical constants were determined for as-deposited films and films heat treated in vacuum at 400 and 500 °C to assess their suitability for utilization in solar-selective surfaces for evacuated collectors and other optical coatings. The materials were fabricated with aluminium, chromium, stainless steel, silicon and titanium post cathodes, and butane, CO, CF_4, N_2 and O_2 reactive gases. In particular, materials based on Al–C–O, Al–C–F and Al–N have deposition parameters and optical properties suitable for solar-selective surfaces. A dielectric material based on Al–C–F has a refractive index n of about 1.4, a low k value and a relatively high deposition rate, and it may be suitable for transparent protective coatings, antireflection coatings or the low refractive index component in multilayer stacks.

1. INTRODUCTION

Reactive sputtering, in which a gas is employed to introduce one or more coating constituents, is a thin film deposition technique which allows the fabrication of a wide range of metal–non-metal composite materials. The reactive sputtering process is complex, involving dissociation and ionization of gas molecules in the plasma and chemical reactions on both the cathode and the surface of the deposited film. Composite materials with a wide range of atomic ratio of metal to non-metal can be deposited by varying the deposition conditions, and a particular composite material can be accurately and repeatedly deposited by reproducing empirically determined sputtering conditions such as cathode current density and reactive gas injection rate. Cylindrical and planar magnetron sputtering technology[1] allows high rate uniform deposition onto large areas and the precise control of deposition parameters because of the highly stable nature of the magnetically confined plasma. D.c. reactively sputtered films produced in cylindrical and planar magnetrons have been developed for applications such as wear-resistant or protective coatings[2],

* Permanent address: Tsinghua University, Beijing, China.

0040-6090/84/$3.00

decorative coatings[3], transparent conducting coatings and transparent heat mirrors[4], solar-selective absorbing surfaces[5], semiconductor devices (*e.g.* photovoltaic cells)[6] and dielectrics[7].

The development of reactively sputtered films for optical coatings such as solar-selective absorbing surfaces requires a detailed knowledge of the optical properties and deposition parameters of the films. Selective absorbing surfaces exhibit the properties of high absorptance for solar wavelengths (0.3–2 μm) and low emittance for thermal IR radiation (2–20 μm) and are usually a tandem of a thin film absorber on a low emittance metal base layer. The fabrication of the absorbing layer of a selective surface requires deposition deep within the absorbing layer of a material with an extinction coefficient $k \approx 1.0$ for solar wavelengths (for absorption of sunlight) and a material at the top surface of the absorbing layer with a low refractive index n (preferably $n < 2.0$) and a low k value (preferably $k < 0.25$) which serves as an antireflection film for the absorbing layer. Maximum solar absorptance is obtained by continuously grading the optical properties of the absorbing layer from a high k material at the low emittance metal base layer to a low n, low k material at the top surface[8]. Reactive sputtering is an excellent method of producing this grading profile because ideally the entire absorbing layer may be produced by sputtering a single metal cathode with a continuously increasing flow of reactive gas to the sputter zone. Graded stainless steel–carbon selective surfaces are fabricated in this way using a stainless steel cathode and acetylene (C_2H_2) as the reactive gas to produce an absorbing layer which varies in composition continuously from carbon-free stainless steel to metal-free amorphous hydrogenated carbon (a-C:H)[9]. Alternatively, an absorbing layer may be constructed by sequential deposition of composite films reactively sputtered using different metal cathodes and different reactive gases. However, this requires the construction of a more complex multielectrode production system.

In addition to the requirements on the optical properties, sputtered materials for selective absorbing surfaces must be stable at the operating temperature of the solar collector. For evacuated solar collectors with typical operating temperatures greater than 100 °C, the selective surface must survive a short (about 1 h) exposure to temperatures of 400–500 °C, which is a necessary part of the collector evacuation process[10]. In this paper we survey the deposition parameters and optical properties of a range of d.c. magnetron reactively sputtered materials, with a view to assessing their potential for solar-selective surfaces in evacuated collectors and for other possible optical applications such as antireflection coatings. The stability of the materials was evaluated by measuring changes in the optical properties after heating to 400 or 500 °C in a vacuum furnace. The materials were fabricated using readily available metals such as aluminium, chromium, stainless steel (type 316) and titanium and constituents from the reactive gases butane (C_4H_{10}), CO, CF_4 (Freon 14), N_2 and O_2. Some additional composite materials were produced using a silicon cathode and N_2 or O_2 as the reactive gas.

2. EXPERIMENTAL DETAILS

Three d.c. post cathode cylindrical magnetron sputtering systems were used in the preparation of the composite materials. Post cathode magnetrons with

elongated cathodes were utilized in this work because of the previous successful development of post cathode magnetron systems for the production coating of elongated tubular solar energy absorbers at Sydney University[11] and Nitto Kohki Co. Ltd. (Tokyo, Japan). System CM1 (Fig. 1) contains a single axial post cathode (25 mm in diameter and 0.28 m long) and rotatable substrate holders distributed around the circumference of the chamber. Sputtering was performed with a cathode current density of 45 A m^{-2}. System CM2 (Fig. 1) contains a single axial post cathode in a vacuum chamber of smaller diameter than that of system CM1. Substrates are introduced via a specimen holder on a slide wire. This system was used exclusively for sputtering a silicon electrode at a current density of 25 A m^{-2}. System CM3 (Fig. 1) is a prototype production system for coating tubular substrates[11]. Planetary motion of the tubular substrates allows tubes to be uniformly coated with material sputtered from either of two post cathodes (38 mm in diameter and 1.7 m long) at a cathode current density of 90 A m^{-2}. Sputtering was performed with a mixture of argon and reactive gas or simply with the reactive gas. In each system argon was introduced via a single gas inlet at the chamber end closest to the diffusion pump. Reactive gas was introduced via pinholes in a gas feed pipe running parallel to the post cathode. The argon pressure used in each of the sputtering chambers was 0.4 Pa, and the magnetic field intensity was about 0.03 T.

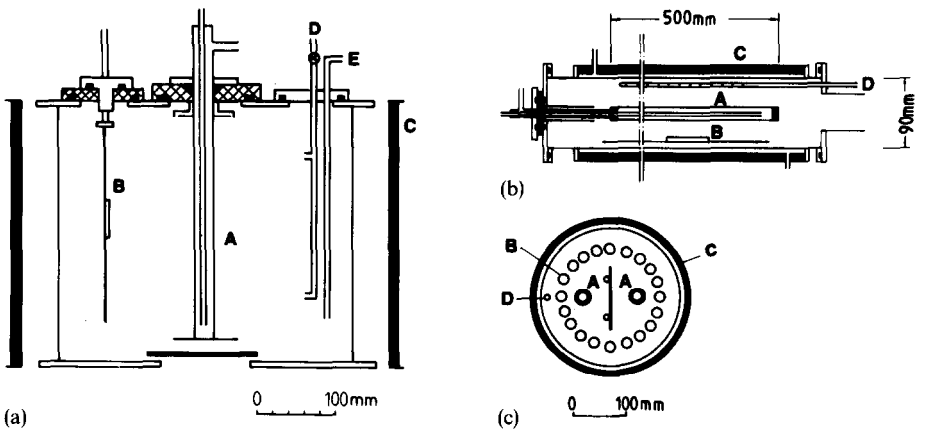

Fig. 1. Schematic diagrams of post cathode cylindrical magnetron sputtering systems CM1 (a), CM2 (b) and CM3 (c) (longitudinal sections are shown for CM1 and CM2; a cross section is shown for CM3): A, post cathode; B, substrates (glass slides or tubes); C, field coil; D, reactive gas inlet; E, argon inlet.

Homogeneous films of thickness greater than 0.4 μm were sputtered onto copper-coated glass substrates (substrate temperature, about 20 °C) for compositional analysis with an electron microprobe (Energy Technology Engineering Center autoprobe, U.S.A.). The compositions of most of the materials were thus determined within about 2 at.% for each element. The compositions of a few thin films were determined by Auger electron spectroscopy using standard elemental sensitivity factors. Uncertainties in these cases may exceed 50% for each element. Homogeneous films of thickness 30–100 nm were sputtered onto clean soda glass substrates, which had pre-sputtered copper strips, for the determination of the

optical constants n and k (where the complex refractive index is $n - ik$) and the sheet electrical resistance at 300 K. The optical constants were determined as a function of wavelength in the range 0.4–2.5 μm from the reflectance and transmittance measured at near-normal incidence. Reflectances and transmittances were measured using a Beckman DK-2A ratio recording spectrophotometer and film thicknesses were measured to within ±2 nm using a Talystep 1 stylus instrument. Initial values for the optical constants n and k were derived from the reflectances and transmittances (corrected for the effect of the glass substrate) by using computer-generated curves of the normal incidence reflectance R and transmittance T *versus* film thickness or wavelength[12]. The initial n and k values were then refined by interactive computer calculation of R and T using the Hadley equations[13]. Any ambiguity in the values of n and k resulting from a single observation of R, T and the thickness or wavelength was resolved by determination of n and k for an alternative thickness. Uncertainties in n and k resulting from uncertainties in film thickness and film reflectance and transmittance varied from ±5% to ±10%, except for the highly absorbing (*i.e.* high k) films where uncertainties were generally higher.

Film thickness, composition, electrical resistivity and optical constants were thus determined for both as-deposited and heat-treated films. Heat treatment involved temperatures of 400 and/or 500 °C for 1 h in a continuously pumped Pyrex vacuum furnace at a pressure of less than 1 mPa. Film deposition rates (in nanometres per kilowatt per second) appropriate to the particular sputtering system used were determined for each composite material from the thickness measurements and cathode power. Relative deposition rates are of importance for industrial production, so the deposition rate from a copper cathode in each sputtering system was used to estimate relative deposition rates on the basis that the deposition rate for pure copper is 1.0.

Metal cathodes were constructed using standard commercially available aluminium tube (purity, 99 at.%), titanium tube (purity, 99.9 at.%), stainless steel tube (type 316) and copper tube with chromium electroplated onto it. A silicon cathode was fabricated using semiconductor-grade doped single-crystal silicon wafers electroplated with nickel and soldered to a copper tube of rectangular cross section (25 mm × 12 mm).

3. PROPERTIES OF REACTIVELY SPUTTERED MATERIALS—RESULTS AND DISCUSSION

The electrical and optical properties of all the as-deposited composite materials generally behaved as expected, with increases in electrical resistivity and decreases in both n and k as the reactive gas flow rate to the sputter zone was increased[14]; also increases (decreases) in k associated with heat treatment were invariably associated with decreases (increases) in the electrical resistivity. Thickness decreases normally occurred in the thin films during heat treatment at 400 or 500 °C. This may in some cases be associated with decomposition of the films, but the sputter gas pressure and cathode–substrate distances employed in sputtering systems CM1 and CM3 correspond to conditions which induce structural porosity, *i.e.* film structures which consist of columnar grains with open boundaries[15]. Consequently, thickness decreases may generally be associated with an increase in packing density during annealing. Compositional results apply to the average properties of the relatively

thick (thicker than 0.4 μm) films required for microprobe analysis. Consequently, compositional changes which may occur during heat treatment of the thin films for measurement of optical properties (*e.g.* changes due to surface oxidation) may not be observed in the compositional analysis of heat-treated thick films. In addition, the composition of as-deposited and heat-treated thin films may be influenced by the glass substrate[16]. No attempt has been made to investigate these possibilities.

An abrupt transition from the metal mode to the dielectric mode with an associated reduction in deposition rate is generally observed for the sputtering of a metal cathode in mixtures of argon and a reactive gas as the reactive gas injection rate is increased for constant cathode power density (ref. 1, p. 108). The transition point occurs when the reactive gas flow is such that a dielectric material is sputtered, and it is associated with the formation of compounds which completely coat the cathode (cathode poisoning). The transition is often accompanied by a sharp decrease in discharge voltage (for constant current) (ref. 1, p. 108). In the present work detailed characteristic curves of cathode voltage *versus* reactive gas flow rate were determined for an aluminium cathode and the reactive gases CF_4, CO, O_2 and N_2.

In the following sections, the properties of the various reactively sputtered composite materials are discussed in detail. Data tabulated for each material include the sputtering system used, the gas pressure, the reactive gas flow (expressed as a proportion of the critical flow at which the transition from the metal mode to the dielectric mode occurs), the film deposition rate per unit power dissipated in the particular sputtering system used, the relative deposition rate (Section 2), the thickness of the films (as deposited and after heat treatment) used to determine the optical constants, the electrical resistivity of the as-deposited and heat-treated films and the composition of thick films deposited under the same conditions as the thin films used for measurement of the optical constants. Optical constants n and k for wavelengths of 0.4–2.5 μm are presented in graphical form. Sample error bars are shown on each graph.

3.1. Aluminium cathode

3.1.1. CF_4 (Freon 14) reactive gas

The properties of four Al–C–F composite materials, AlCF1–AlCF4, are summarized in Table I and Fig. 2. In determining compositions, a low electron beam power was required to avoid decomposition during electron microprobe analysis. These materials contain some O_2 impurity from residual gas in the sputtering system.

Relatively high deposition rates are obtained for AlCF1–AlCF3, and an anomalously high rate is obtained for the dielectric AlCF4. Figure 3 shows a graph of discharge voltage *versus* relative flow rate of CF_4 to the sputter zone, where a relative flow rate of 1.0 corresponds to the deposition of dielectric material. The results indicate that an anomalous sharp decrease in voltage occurs at a relative flow rate of 1.7. A material AlCF5 was prepared at a relative flow rate of 2.3 (*i.e.* a flow rate beyond the voltage anomaly) for comparison with AlCF4 (which was prepared at a relative flow rate of 1.0). Deposition rates were identical for the two materials and compositions were nearly identical (see Table I), the Al:F atomic ratio being close to 1:3.

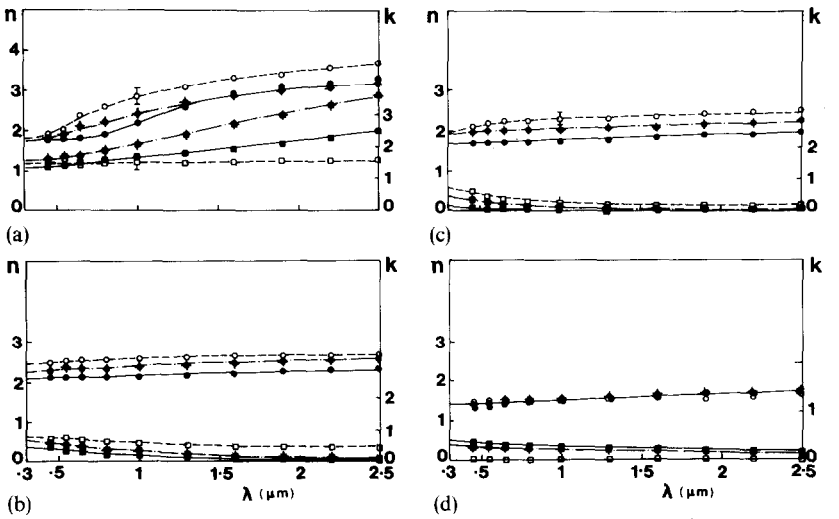

Fig. 2. Refractive index n (○, ●, ◆) and extinction coefficient k (□, ■, ◆) *vs.* wavelength λ for the homogeneous Al–C–F films ((a) AlCF1; (b) AlCF2; (c) AlCF3; (d) AlCF4) described in Table I: ○, □, as-deposited films; ●, ■, heat-treated films (1 h at 500 °C); ◆, ◆, heat-treated films (1 h at 400 °C).

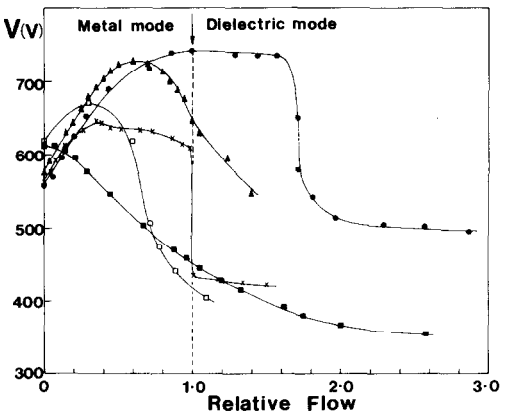

Fig. 3. Characteristic curves of cathode voltage *vs.* reactive gas relative flow rate for an aluminium post cathode sputtered in argon–reactive gas mixtures: —●—, CF_4 (CM1); —▲—, CO (CM1); —×—, O_2 (CM1); —■—, N_2 (CM1); —□—, N_2 (CM3). A relative flow rate of 1.0 results in deposition of dielectric material.

The high deposition rates for AlCF4 and AlCF5 suggest that plasma etching occurs at the cathode and possibly deposition of carbon and fluorine occurs directly from the magnetron glow discharge because of a tendency for carbon-based reactive species to polymerize on the substrate surface. Sputtering at high flow rates of CF_4 is therefore somewhat similar to sputtering at high flow rates of a hydrocarbon (*e.g.* C_2H_2)[9]; however, in the former case a significant amount of metal is incorporated in the film, whereas in the latter case metal-free hydrogenated carbon may be deposited (Section 3.4.1).

Large increases in resistivity and decreases in n and k occur for AlCF2 and AlCF3 during heat treatment, possibly as a result of oxidation of aluminium in the

films by residual water vapour in the furnace (the optical constants for Al_2O_3 are $n \approx 1.7$ and $k = 0$). The index n for AlCF4 is unchanged after heat treatment, but k increases significantly. The decrease in thickness for AlCF4 during heat treatment is particularly large (about 20%) indicating partial decomposition. This has been confirmed by gas evolution studies currently in progress here[17] which show that small amounts of CO, flourine, CF and CF_3 are evolved from the material AlCF4. This decomposition may increase the number density of aluminium atoms bonded in a metal rather than a metal–non-metal phase. An equivalent mechanism is a structural change involving a decrease in carbon–metal bonding states which has been observed during heat treatment of sputtered metal–carbon materials[18,19]. The consequent increase in the density of electron states in the conduction band[20] results in an increase in the extinction coefficient k.

The possibility of grading the optical properties of Al–C–F materials from highly absorbing (AlCF1) to highly transparent with a low index n (AlCF4) suggests the suitability of this material for graded selective absorbing surfaces. The property of considerable interest for material AlCF4 is the low index n of about 1.4 for visible wavelengths. This refractive index value is typical of evaporated AlF_3 which has been utilized in optical coatings[21]. The low n value is ideal for antireflection coatings but the finite k value after heat treatment at temperatures of 400 or 500 °C may be a disadvantage; however, the extinction coefficient k has been found to undergo negligible change for temperatures up to about 200 °C. The magnitude of k for as-deposited films has been determined from transmittance and reflectance measurements on relatively thick (more than 0.4 μm) films. Results are summarized in Table II. The extinction coefficients obtained here are probably too high for some optical coatings but the deposition conditions have not been optimized. The adhesion and abrasion resistance of this material appears to be reasonably good in contrast with the properties of an Mg–C–F material (produced by sputtering magnesium in argon plus CF_4) produced by Coleman[16].

3.1.2. CO reactive gas

The properties of three Al–C–O composite materials, AlCO1–AlCO3, are summarized in Table I and Fig. 4. The compositional changes which occur during heat treatment are minor. The material AlCO3 which is sputtered using CO (no argon) contains about 4 at.% metal and thus consists predominantly of a single phase of an oxygenated carbon matrix with a small concentration of aluminium carbide, aluminium oxide or aluminium metal particles. This is similar to the structure observed for some metal–carbon materials[18]. The considerable decrease in deposition rate for AlCO3 compared with AlCO1 and AlCO2 is typical of the transition from the metal mode to the dielectric mode (ref. 1, p. 108). The deposition rate of carbon and oxygen from the glow discharge is apparently relatively low because of their inability to polymerize. The variation in discharge voltage with CO flow rate to the sputter zone (for constant current) is shown in Fig. 3. Dielectric material is produced for a relative flow rate of 1.0. No sharp decrease in discharge voltage is observed in this case.

The decreases in n and k associated with heat treatment of AlCO1 and AlCO2 are probably associated with oxidation of aluminium carbide or aluminium metal particles in the film. The oxygen derives from the oxygenated carbon which evolves CO gas at temperatures above 400 °C[17]. The compositions shown in Table I

TABLE I

DEPOSITION PARAMETERS AND FILM PROPERTIES FOR MATERIALS PRODUCED BY REACTIVE SPUTTERING OF AN ALUMINIUM CATHODE

Material	*Sputtering system*	*Argon pressure* (Pa)	*Reactive gas flow* (arbitrary units)	*Deposition rate* ($nm\ s^{-1}\ kW^{-1}$)	*Relative deposition rate*	*Film status*	*Film thickness* (nm)	*Resistivity* ρ (Ω m)	*Composition of thick (greater than 0.4 μm) films* (at.%)				
									Al	*C*	*F*	*O*	*N*
AlCF1	CM1	0.4	0.37	0.87	0.59	AD	34	2×10^{-5}	38	33	28		
						HT400	31	2×10^{-5}					
						HT500	31	7×10^{-5}					
AlCF2	CM1	0.4	0.63	0.78	0.53	AD	33	5×10^{-4}	33	33	33		
						HT400	30	> 2.0					
						HT500	33	> 2.0					
AlCF3	CM1	0.4	0.85	0.78	0.53	AD	33	1×10^{-2}	28	33	38		
						HT400	30	> 2.0					
						HT500	35	> 2.0					
AlCF4	CM1	0.4	1.0	1.05	0.71	AD	100	> 2.0	23	8	66	2	
						HT400	84	> 2.0					
						HT500	80	> 2.0					
AlCF5	CM1	0.4	2.3	1.05	0.71	AD		> 2.0	21	12	65	2	
AlCO1	CM1	0.4	0.25	0.72	0.49	AD	31	2×10^{-5}					
						HT500	32	> 2.0					
AlCO2	CM1	0.4	0.87	0.68	0.46	AD	39	2×10^{-4}	23	68		8	
						HT500	38	> 2.0	23	71		5	
AlCO3	CM1	0 ($P_{CO} = 0.4$)	2.5	0.23	0.16	AD	80	> 2.0	4	77		18	
						HT500	65	> 2.0	4	73		22	
AlN1	CM1	0.4	0.50	0.70	0.47	AD	21	4×10^{-6}	68			2	29
						HT500	22	5×10^{-6}	68			2	29
AlN2	CM1	0.4	0.63	1.05	0.71	AD	30	2×10^{-5}	57			3	39
						HT400	25	3×10^{-5}					
						HT500	26	> 2.0	57			2	39
AlN3	CM1	0.4	0.88	0.80	0.54	AD	40	2×10^{-2}	49			2	48
						HT400	40	0.7					
						HT500	41	> 2.0	52			3	44

(continued)

TABLE I *(continued)*

Material	*Sputtering system*	*Argon pressure* (Pa)	*Reactive gas flow* (arbitrary units)	*Deposition rate* ($nm\ s^{-1}\ kW^{-1}$)	*Relative deposition rate*	*Film status*	*Film thickness* (nm)	*Resistivity* ρ (Ω m)	*Composition of thick (greater than 0.4 μm) films* (at.%)				
									Al	*C*	*F*	*O*	*N*
AlN4	CM1	0 ($P_{N_2} = 0.4$)	3.0	0.17	0.12	AD	45	> 2.0	38			3	58
						HT500	42	> 2.0	38			2	59
AlN5	CM1	0 ($P_{N_2} = 1.5$)	3.0	0.17	0.12	AD	87	> 2.0	≈ 50			≈ 40	≈ 10
						HT500	87	> 2.0					
AlO_x	CM1	0 ($P_{O_2} = 0.4$)	1.5	0.07	0.04	AD	84	> 2.0	≈ 50			≈ 50	
						HT500	73	> 2.0					

The reactive gas flow is expressed as a fraction of the flow for which the transition from the metal mode to the dielectric mode occurs. The relative deposition rate was determined by comparison with the deposition rate for pure copper metal. The film status is described as follows: AD, as deposited; HT400, heat treated in vacuum for about 1 h at 400 °C; HT500, heat treated in vacuum for about 1 h at 500 °C. Thicknesses are those for the films used to determine optical constants. The compositions of materials AlN5 and AlO_x were estimated from Auger electron spectroscopy data using standard elemental sensitivity factors.

TABLE II

EXTINCTION COEFFICIENTS k DETERMINED FROM REFLECTANCE AND TRANSMITTANCE MEASUREMENTS ON VARIOUS THICK (ABOUT 0.5 μm) FILMS

Material		*Extinction coefficient at various wavelengths*			
		0.45 μm	*0.55 μm*	*0.65 μm*	*1.00 μm*
AlCF4	AD[a]	0.008 ± 0.003	0.005 ± 0.003	0.004 ± 0.003	0.002 ± 0.001
AlN4	AD[a]	0.010 ± 0.001	0.005 ± 0.001	0.004 ± 0.002	0.002 ± 0.002
	HT[a]	0.008 ± 0.001	0.006 ± 0.002	0.006 ± 0.002	0.004 ± 0.002
AlO_x	AD[a]	0.006 ± 0.001	0.004 ± 0.002	0.003 ± 0.002	0.003 ± 0.003
	HT[a]	0.007 ± 0.001	0.006 ± 0.002	0.004 ± 0.002	0.002 ± 0.002

[a] AD, as-deposited; HT, heat treated in vacuum for 1 h at 500 °C.

confirm that a net decrease in oxygen content occurs during heat treatment of AlCO2 as a result of the evolution of CO gas. The sharply increasing k values at short wavelengths for as-deposited and heat-treated AlCO3 suggest the existence of an energy gap associated with oxygenated carbon, similar to energy gaps observed in semiconductors such as hydrogenated carbon and silicon[22,23]. The k value also increases sharply at short wavelengths for heat-treated AlCO2. There may similarly be some contribution to k from an oxygenated carbon matrix in this material; however, the properties of AlCO2 are complicated by the presence of a significant proportion of at least one other phase (aluminium carbide, oxide or aluminium metal). Thus the behaviour of k may result predominantly from Maxwell Garnett absorption associated with conducting particles in the oxygenated carbon matrix[18].

Figure 5 shows a graph of $(nk)^{1/2}/\lambda$ *versus* photon energy $h\nu$ (where λ is the wavelength) for the as-deposited and heat-treated AlCO3 films. The intercepts of the extrapolated linear portions of these graphs with the photon energy axis give an estimate of the energy intercept E_g for the as-deposited and heat-treated films[24]. The intercepts obtained from such graphs for heat-treated AlCO2 and as-deposited and heat-treated AlCO3 are summarized in Table III. The low value of the intercept obtained for heat-treated AlCO2, compared with that for AlCO3, suggests that

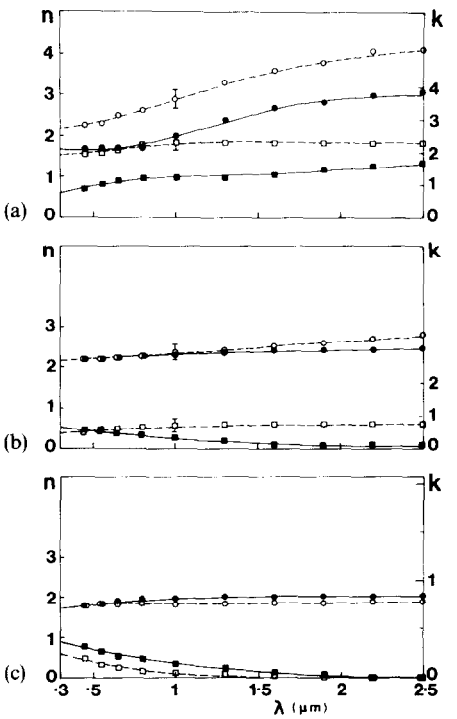

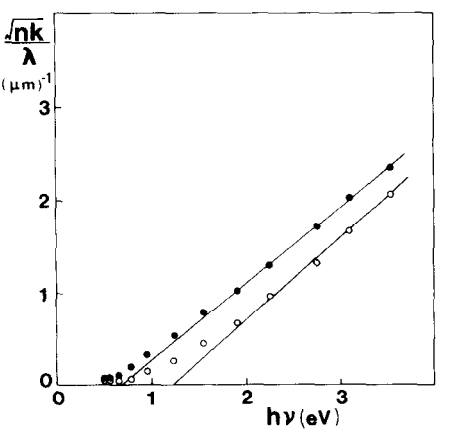

Fig. 4. Refractive index n (○, ●) and extinction coefficient k (□, ■) *vs.* wavelength λ for the homogeneous Al–C–O films ((a) AlCO1; (b) AlCO2; (c) AlCO3) described in Table I: ○, □, as-deposited films; ●, ■, heat-treated films (1 h at 500 °C).

Fig. 5. Graphs of $(nk)^{1/2}/\lambda$ *vs.* photon energy $h\nu$ used to determine the energy band gap of as-deposited (—○—) and heat-treated (—●—) material AlCO3.

TABLE III
ENERGY INTERCEPT E_g DETERMINED FOR VARIOUS COMPOSITE MATERIALS (SEE FIG. 5)

Material	*Energy intercept E_g of the sample* (eV)	
	As deposited	*Heat treated (1 h in vacuum at 500 °C)*
AlCO2	—	0.4±0.1
AlCO3	1.2±0.1	0.7±0.1
CrO3	1.4±0.1	1.3±0.1
a-C:H (C_4H_{10})	1.8±0.2	1.4±0.1
SSCO6	0.7±0.2	0.4±0.2
SSO4	1.7±0.1	1.4±0.1
TiCO3	1.1±0.1	0.8±0.1

absorption in AlCO2 is predominantly associated with Maxwell Garnett absorption, whereas the k value for AlCO3 is predominantly associated with the oxygenated carbon matrix, with a smaller contribution from Maxwell Garnett absorption associated with the impurity phase.

As proposed in previous work on a-C:H [25], evolution of CO from amorphous carbon will result in an increase in the number density of C=C double bonds in the network, with a consequent decrease in the energy intercept E_g as observed for AlCO3. The significant decrease in thickness of AlCO3 and gas evolution work[17] confirm that substantial decomposition occurs. A decreased resistivity of the impurity phase after heat treatment (see Section 3.1.1), with an associated increase in Maxwell Garnett absorption, will also contribute to the decrease in the energy intercept.

The optical properties of these composite materials suggest that they may be utilized in a graded selective surface. The material AlCO3 is characterized by a moderately low n value (about 1.9–2.0) and a reasonably low k value (about 0.3) for visible wavelengths and so is acceptable as an antireflection layer.

3.1.3. N_2 reactive gas

Reactively sputtered Al–N composite materials have been studied previously as dielectric materials and for surface acoustic wave devices[7,26].

The properties of four Al–N composite materials (AlN1–AlN4) are summarized in Table I and Fig. 6. A few atomic per cent of oxygen is present in all the films because of residual gas in the sputtering chamber. The compositional changes which occur during heat treatment are minor. The composition of the material AlN4 is close to that of Al_2N_3, in contrast with the stoichiometry AlN usually claimed for dielectric aluminium nitride[26]. The deposition rate for AlN4 is considerably lower than those for AlN1–AlN3 as a consequence of the transition from the metal mode to the dielectric mode (ref. 1, p. 108). The variation in discharge voltage with flow rate of N_2 to the sputter zone of CM1 is shown in Fig. 3. (A relative flow rate of 1.0 corresponds to deposition of dielectric material.) Similar to aluminium sputtered with CO gas, no sharp decrease in voltage occurs; however, this behaviour seems to be typical for metals sputtered in Ar–N_2 mixtures (ref. 1, p. 108). Results are also shown for aluminium sputtered in Ar–N_2 mixtures in the production coating system CM3. The voltage *versus* gas flow rate characteristic differs in that a pronounced

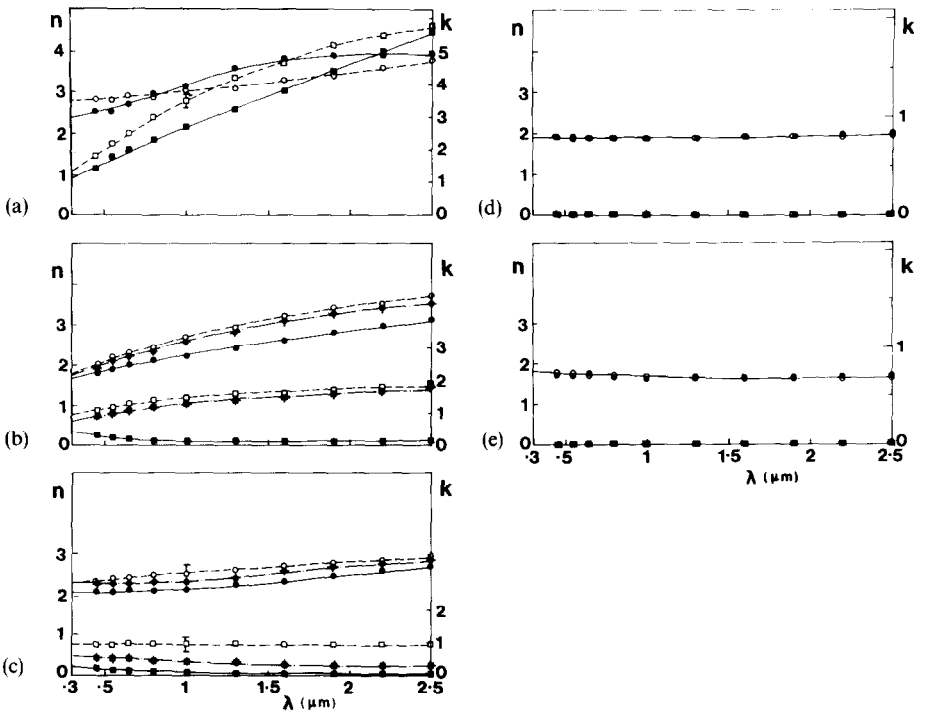

Fig. 6. Refractive index n (○, ●, ✦) and extinction coefficient k (□, ■, ✦) *vs.* wavelength λ for the homogeneous Al–N films ((a) AlN1; (b) AlN2; (c) AlN3; (d) AlN4; (e) AlN5) described in Table I: ○, □, as-deposited films; ●, ■, heat-treated films (1 h at 500 °C); ✦, ✦, heat-treated films (1 h at 400 °C).

peak occurs in voltage for relatively low flow rates. Thus this characteristic is somewhat dependent on the geometry of the sputtering system. Decreases in n and k which occur during heat treatment of AlN1–AlN3 are probably associated with oxidation of the thin films by residual water vapour in the furnace, with the formation of Al_2O_3 in the films.

The value $n \approx 1.9$ for material AlN4 for visible wavelengths is in reasonable agreement with the values 1.7–1.9 reported elsewhere for films of AlN prepared by d.c. planar magnetron sputtering[7]. AlN is an insulator with a band gap of about 6 eV [7,27] and consequently should exhibit an extremely low extinction coefficient. The magnitude of k for our as-deposited and heat-treated films was determined from transmittance and reflectance measurements on relatively thick (greater than 0.4 μm) films (see Table II). The k values are quite low, although deposition conditions have not been optimized. Both n and k are unaffected by heat treatment at 500 °C because of the refractory nature of AlN which has a decomposition temperature of about 2500 °C [7]. Gas evolution studies show that N_2 is evolved from AlN4 near 500 °C [17]. This instability is probably associated with the excess nitrogen contained in AlN4 (see Table I).

The optical properties of composite materials AlN1–AlN4 suggest that they are suitable for the fabrication of the absorbing layer of a selective surface. The material AlN4 has a moderately low n value and a negligible k value and is therefore suitable as

an antireflection layer. Selective surfaces incorporating a graded Al–N absorbing layer with a solar absorptance exceeding 0.92 have recently been fabricated in sputtering system CM3. Preliminary results are presented elsewhere[28].

A material AlN5 (see Table I and Fig. 6) has been deposited by sputtering aluminium in N_2 (no argon) at a pressure of about 1.5 Pa with a view to depositing the material with a lower packing density and a resultant lower refractive index[29–31]. Figure 6 shows that values of $n \approx 1.75$ and $k \approx 0$ are obtained for AlN5 with no loss of deposition rate (Table I). This material has a small advantage over AlN4 as an antireflection layer. The reduced n value is probably partly associated with the development of structure in the film; however, Auger analysis has indicated an extremely high oxygen content (see Table I) as a result of a higher partial pressure of residual water vapour in the sputter zone which is present because of the increased throttling of the diffusion pump necessary to increase N_2 pressure in the chamber. The high oxide content of AlN5 is probably primarily responsible for the decrease in n because of the low index of Al_2O_3 ($n \approx 1.7$). The deposition rate of AlN5 is three times that of aluminium oxide produced by sputtering aluminium in pure O_2 (Section 3.1.4 and Table I). The high rate is apparently associated with the presence of N_2 in the sputter gas. This effect has been observed for other reactively sputtered oxides[32].

3.1.4. O_2 reactive gas

Considerable difficulty has been experienced in producing Al–O composite materials with a continuous range of optical properties because of the abrupt transition from the metal mode to the dielectric mode which occurs when a critical O_2 partial pressure is exceeded. Figure 3 shows that an abrupt voltage decrease is associated with this transition.

Al–O composite materials with a continuous range of optical properties have not been prepared. However, aluminium oxide produced by sputtering aluminium in O_2 (no argon) has suitable optical properties for an antireflection layer. Evaporated and sputtered aluminium oxide of stoichiometry close to Al_2O_3 shows $n \approx 1.70$ and has been used extensively in selective absorbing surfaces[33–35].

The properties of an Al–O composite material (AlO_x) produced by sputtering aluminium in O_2 (no argon) are summarized in Table I and Fig. 7. The composition of this material was analysed by Auger depth profiling which gave a composition close to AlO (Table I), but the values $n \approx 1.7$ and $k \approx 0$ are typical of Al_2O_3. Values of k obtained from measurements on thick (greater than 0.4 μm) films are shown in Table II. No changes occur in composition or optical constants during heat treatment at 500 °C. A major problem for mass production of this material is the low deposition rate; however, enhanced rates may be possible by sputtering in O_2 plus N_2 (see Section 3.1.3 and ref. 32).

3.2. Chromium cathode

3.2.1. O_2 reactive gas

The properties of three Cr–O composite materials, CrO1–CrO3, are summarized in Table IV and Fig. 8(a). Because of the abrupt transition from the metal mode to the dielectric mode which occurs when a critical O_2 partial pressure is exceeded, deposition of a homogeneous material with optical properties intermediate between CrO2 and CrO3 proved to be impossible. Similar problems with

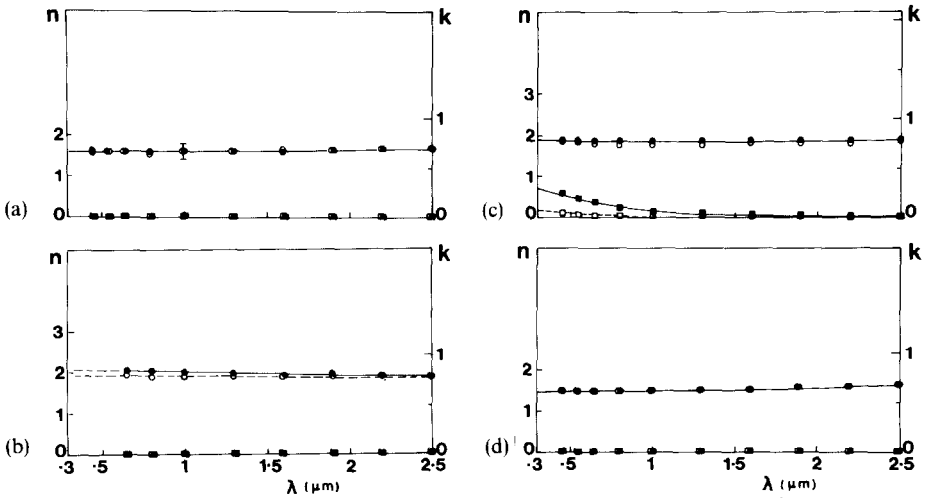

Fig. 7. Refractive index n (○, ●) and extinction coefficient k (□, ■) *vs.* wavelength λ for the homogeneous films ((a) AlO_x; (b) SiN_x; (c) a-C:H (C_4H_{10}); (d) SiO_x) described in Tables I, V and VI: ○, □, as-deposited films; ●, ■, heat-treated films (1 h at 500 °C).

TABLE IV

DEPOSITION PARAMETERS AND FILM PROPERTIES FOR MATERIALS PRODUCED BY REACTIVE SPUTTERING OF A CHROMIUM CATHODE IN ARGON PLUS O_2 (SEE TABLE I FOOTNOTE FOR DETAILS)

	CrO1		*CrO2*		*CrO3*	
	AD	*HT500*	*AD*	*HT500*	*AD*	*HT500*
Sputtering system	CM1	CM1	CM1	CM1	CM1	CM1
Argon pressure (Pa)	0.4	0.4	0.4	0.4	0	0
					$P_{O_2} = 0.4$	$P_{O_2} = 0.4$
Reactive gas flow (arbitrary units)	0.92	0.92	0.96	0.96	2.5	2.5
Deposition rate (nm s^{-1} kW^{-1})	0.83	0.83	0.83	0.83	0.22	0.22
Relative deposition rate	0.56	0.56	0.56	0.56	0.14	0.14
Film thickness (nm)	45	43	44	40	67	46
Resistivity ρ (Ω m)	4×10^{-6}	4×10^{-6}	2×10^{-5}	2×10^{-5}	> 2.0	> 2.0
Composition of thick (greater than 0.4 μm) films (at.%)						
Cr	88	88	79	67	33	34
O	10	10	20	31	65	65

Cr–O materials were encountered by Thornton[30]. The composition of the dielectric material CrO3 is close to that of CrO_2, which contrasts with the stoichiometry Cr_2O_3 usually assumed for dielectric chromium oxide; however, evidence for CrO_2 in d.c. reactively sputtered chromium oxide has been obtained from X-ray diffraction measurements[36]. The compositions of CrO1 and CrO3 are unaffected by heat treatment at 500 °C although the large thickness decrease of CrO3 during heat treatment indicates a tendency for this material to sublime partially. The deposition rate of CrO3 is low compared with those of CrO1 and CrO2, as a consequence of the transition from the metal mode to the dielectric mode.

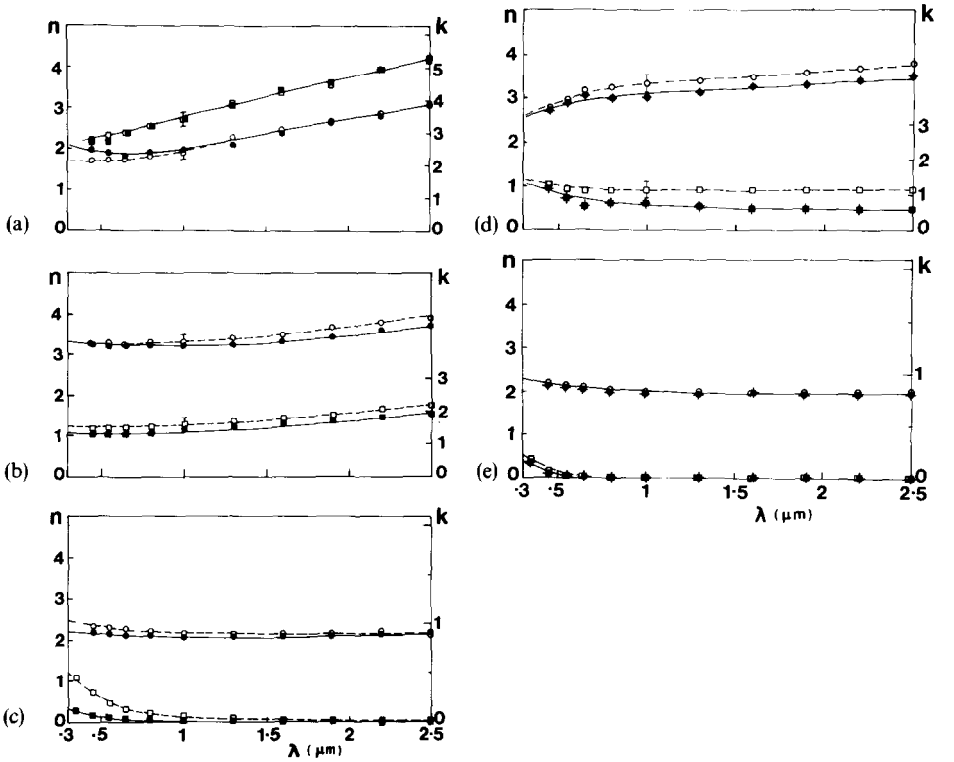

Fig. 8. (a)–(c) Refractive index n (○, ●, ✦) and extinction coefficient k (□, ■, ✦) *vs.* wavelength λ for the homogeneous Cr–O films ((a) CrO1; (b) CrO2; (c) CrO3) described in Table IV. (d), (e) Refractive index for evaporated Cr–O films ((d) E-CrO1; (e) E-CrO2): ○, □, as-deposited films; ●, ■, heat-treated films (1 h at 500 °C); ✦, ✦, heat-treated films (1 h at 400 °C).

The optical constants of CrO1 and CrO2 are unaffected by heat treatment. Identical results for the optical constants of an as-deposited material produced under similar conditions to CrO3 have been obtained for visible wavelengths by Thornton[30]. The sharply increasing k associated with the predominantly single-phase material CrO3 as the wavelength decreases indicates the existence of an energy band gap. The results of an analysis similar to that performed for AlCO3 (see Section 3.1.2) are summarized in Table III. The energy gap is almost unchanged after heat treatment.

Reactively sputtered Cr–O composite materials are not very suitable for selective absorbing surfaces because of the difficulty in producing a continuous range of optical properties and because CrO3 has a relatively high n value (about 2.2) which is unsuitable for an antireflection layer. The tendency for CrO3 to sublime is also a problem.

Cr–O composite materials produced by r.f. sputtering of separate chromium and Cr_2O_3 targets have been used to fabricate selective surfaces[37]. This deposition technique allows the preparation of a continuous range of cermet materials from pure chromium to pure Cr_2O_3. Two-layer absorbing films were produced consisting of a Cr–Cr_2O_3 cermet ($n \approx 2.5$ and $k \approx 1.0$ for visible wavelengths) and a Cr_2O_3

($n \approx 2.2$ and $k \approx 0$) antireflection layer; however, this deposition technique is not suitable for mass production.

Reactive evaporation also allows the preparation of films with a continuous range of optical properties. Selective surfaces consisting of graded and two-layer Cr–O composite materials produced by reactive evaporation have been developed at Owens, IL, U.S.A., and Tsinghua University, Beijing, China, respectively. The optical properties of the optimum materials utilized in the two-layer surface (Tsinghua), samples E-CrO1 and E-CrO2, are shown in Figs. 8(d) and 8(e) for comparison with the reactively sputtered materials (Figs. 8(a)–8(c)). The material E-CrO1 (the absorbing layer of the selective surface) has lower n and k values than CrO2, and E-CrO2 has lower n and k values than CrO3, so that these reactively evaporated materials (particularly the antireflection layer E-CrO2) are more suited for selective absorbing surfaces than the sputtered Cr–O materials studied here.

3.3. Silicon cathode

3.3.1. O_2 reactive gas

SiO_2 with $n \approx 1.5$, $k \approx 0$ and high stability has ideal optical properties as an antireflection layer and has been utilized in some evaporated[38–40] and sputtered[41] selective surfaces. We have examined an Si–O composite material solely with a view to its use in antireflection layers.

The properties of an Si–O composite material (SiO_x) produced by sputtering a silicon cathode in O_2 (no argon) are summarized in Table V and Fig. 7. The composition of the material is similar to that of SiO_2, with a small oxygen excess. This material is extremely stable, with optical constants similar to those of SiO_2 and a deposition rate approximately four times greater than that for AlO_x.

3.3.2. N_2 reactive gas

Si_3N_4 with $n \approx 2.0$, $k \approx 0$ and high stability has acceptable properties as an antireflection layer and has been utilized in chemically vapour-deposited selective

TABLE V

DEPOSITION PARAMETERS AND FILM PROPERTIES FOR MATERIALS PRODUCED BY REACTIVE SPUTTERING OF A SILICON CATHODE (SEE TABLE I FOOTNOTE FOR DETAILS)

	SiO_x		SiN_x	
	AD	*HT500*	*AD*	*HT500*
Sputtering system	CM2	CM2	CM2	CM2
Argon pressure (Pa)	0	0	0	0
	$P_{O_2} = 0.5$	$P_{O_2} = 0.5$	$P_{N_2} = 0.5$	$P_{N_2} = 0.5$
Deposition rate (nm s^{-1} kW^{-1})	1.12	1.12	1.25	1.25
Relative deposition rate	0.18	0.18	0.20	0.20
Film thickness (nm)	84	80	85	85
Resistivity ρ (Ωm)	> 2.0	> 2.0	> 2.0	> 2.0
Composition of thick (greater than 0.4 μm) films (at.%)				
Si	31	31	20	25
O	68	68	11	10
N			68	64

surfaces[38,42]. R.f. reactively sputtered Si_3N_4 has also been proposed for selective surfaces[43].

In the present work an Si–N composite material (SiN_x) was examined solely with a view to its use as an antireflection layer.

The properties of an Si–N composite material (SiN_x) produced by sputtering a silicon cathode in N_2 (no argon) are summarized in Table V and Fig. 7. This material contains a significant atomic percentage of oxygen as a result of the high reactivity of silicon with residual water vapour in the sputtering chamber. In addition, the nitrogen content is considerably higher than that expected from the stoichiometry Si_3N_4; however, the optical constants ($n \approx 2.0$ and $k = 0$) are comparable with those of Si_3N_4. This sputtered material is quite stable, with a relatively high deposition rate similar to that of SiO_x.

3.4. Stainless steel cathode

3.4.1. C_4H_{10} reactive gas

An intensive study of stainless steel–carbon composite materials produced by sputtering a stainless steel cathode in C_2H_2 and argon has recently been completed[9–11,14,18,19,25,31,44]. For high C_2H_2 partial pressures, metal-free a-C:H is produced by a combination of sputtering from a carbon-coated (*i.e.* "poisoned") cathode and deposition from the glow discharge. The hydrogenated carbon, with $n \approx 1.9$, constitutes an acceptable antireflection layer for stainless steel–carbon selective surfaces. As-deposited films of the hydrogenated carbon show $k < 0.15$ for visible wavelengths, associated with a semiconductor energy gap of about 2 eV[25]. Heat treatment at 500 °C results in H_2 and CO evolution from the films with a resultant decrease in the energy gap to about 1.35 eV and an increased k value (about 0.4) for visible wavelengths. The absorptance of the heat-treated stainless steel–carbon selective surface is limited to about 0.93 by the relatively high h and k values of the hydrogenated carbon antireflection layer[9].

In this work, C_4H_{10} was used with a view to increasing the H:C atomic ratio in both as-deposited and heat-treated films of hydrogenated carbon, which may result in a larger energy gap and a reduced k value for visible wavelengths. The properties of a-C:H produced by sputtering a stainless steel cathode in C_4H_{10} plus argon are summarized in Table III, Table VI and Fig. 7. The refractive index n of a-C:H from C_4H_{10} is identical with that of a-C:H from C_2H_2. The extinction coefficient of as-deposited a-C:H from C_4H_{10} is marginally less than that of a-C:H from C_2H_2; however, the k values are comparable after heat treatment. The energy gaps (Table III) for a-C:H from C_4H_{10} are comparable with those measured for a-C:H from C_2H_2. Consequently sputtering in C_4H_{10} offers no advantages over sputtering in C_2H_2. Possibly a fundamental upper limit to the H:C ratio in the material and to the magnitude of the energy gap is attained by sputtering in either C_2H_2 or C_4H_{10}.

3.4.2. CF_4 reactive gas

The properties of a stainless steel–carbon–fluorine (SSCF) composite material are summarized in Table VI and Fig. 9. This material was investigated to determine whether alternative metals to aluminium could be used to fabricate low index materials. The as-deposited material SSCF exhibits a relatively low n value (about 1.6) and $k \approx 0$, but heat treatment causes a significant decrease in thickness (Table VI) and a significant increase in the values of n and k.

TABLE VI

DEPOSITION PARAMETERS AND FILM PROPERTIES FOR MATERIALS PRODUCED BY REACTIVE SPUTTERING OF A STAINLESS STEEL (TYPE 316) CATHODE (SEE TABLE I FOOTNOTE FOR DETAILS)

Specimen	*Sputtering system*	*Argon pressure* (Pa)	*Reactive gas flow* (arbitrary units)	*Deposition rate* ($nm\ s^{-1}\ kW^{-1}$)	*Relative deposition rate*	*Film status*	*Film thickness* (nm)	*Resistivity* ρ (Ω m)	*Composition of thick (greater than 0.4 μm) films* (at.%)		
									M[a]	*C*	*O*
a-C:H	CM3	0.4	1.0	0.03	0.51	AD	74	> 2.0			
						HT500	65	> 2.0			
SSCF	CM1	0.4	1.2	0.80	0.54	AD	93	> 2.0			
						HT500	63	> 2.0			
SSCO1	CM3	0.4	0.3	0.03	0.42	AD	27	6×10^{-6}	54	29	15
						HT500	24	3×10^{-6}	54	29	15
SSCO2	CM3	0.4	0.5	0.02	0.37	AD	43	1×10^{-5}	46	34	19
						HT500	41	3×10^{-6}	44	37	19
SSCO3	CM3	0.4	0.7	0.02	0.37	AD	36	4×10^{-5}	39	36	24
						HT500	35	7×10^{-6}	43	34	22
SSCO4	CM3	0.4	0.91	0.02	0.39	AD	44	1.9×10^{-4}	32	39	28
						HT500	36	1.1×10^{-4}	33	43	24
SSCO5	CM3	0.4	0.96	0.02	0.37	AD	38	3.6×10^{-4}	24	42	33
						HT500	48	1.4×10^{-3}	26	40	32
SSCO6	CM3	0 ($P_{CO} = 0.4$)	1.0	0.02	0.32	AD	53	> 2	17	51	31
						HT500	52	1.9	20	50	28
SSO1	CM3	0.4	0.34	0.05	0.79	AD	44	9×10^{-6}	77		22
						HT500	42	2×10^{-6}	74		25
SSO2	CM3	0.4	0.59	0.06	0.87	AD	43	4×10^{-5}	65		34
						HT500	38	7×10^{-4}	68		31
SSO3	CM3	0.4	0.88	0.06	0.87	AD	52	3×10^{-3}	52		47
						HT500	48	8×10^{-3}	60		39
SSO4	CM3	0 ($P_{O_2} = 0.4$)	1.25	0.01	0.09	AD	68	> 2.0	39		60
						HT500	62	> 2.0	39		60

[a] M = Fe + Cr + Ni.

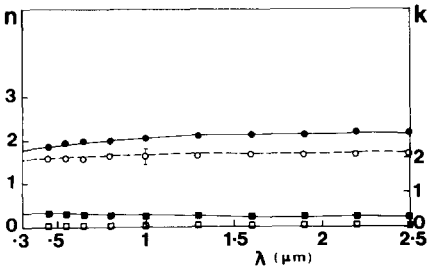

Fig. 9. Refractive index n (○, ●) and extinction coefficient k (□, ■) *vs.* wavelength λ for a homogeneous stainless steel–carbon–fluorine film described in Table VI: ○, □, as-deposited films; ●, ■, heat-treated films (1 h at 500 °C).

3.4.3. CO reactive gas

The properties of six stainless steel–carbon–oxygen composite materials (SSCO1–SSCO6) are summarized in Table VI and Fig. 10. The optical properties of a thin film of pure stainless steel are also shown[9]. The compositions of the materials are not significantly affected by heat treatment; however, CO evolution occurs from these materials near 500 °C [17]. The dielectric material SSCO6 has a high metal content compared with AlCO3. This may be associated with a less pronounced transition from the metal mode to the dielectric mode for stainless steel–carbon–oxygen materials, which allows a continuous range of optical properties to be produced without difficulty and which results in a high deposition rate for SSCO6.

The optical properties are similar to those of stainless steel–carbon materials produced by sputtering stainless steel in C_2H_2 plus argon[9]. Heat treatment has relatively little effect on the index n but results in increases in k for SSCO1–SSCO4. There is an associated decrease in electrical resistivity for these films (Table VI). The changes in optical and electrical properties are probably associated with alterations in the chemical bonding of the metal atoms during heat treatment, as observed for stainless steel–carbon films produced using C_2H_2 (see Section 3.1.1 and refs. 18 and 19). Negligible change occurs in the extinction coefficient of SSCO5 during heat treatment, but the resistivity of this material increases.

Composite material SSCO6 contains about 20 at.% metal (Table VI), and so consists of an oxygenated carbon matrix with a significant amount of metal carbide, metal oxide or metal particle impurity, similar to AlCO2. Almost identical n and k values have been measured by Thornton[30] for an as-deposited material produced under similar conditions to those for SSCO6. The extinction coefficient of SSCO6 depends strongly on wavelength. An analysis similar to that illustrated in Fig. 5 produced the energy intercepts summarized in Table III. The energy intercepts for as-deposited and heat-treated SSCO6 are considerably smaller than for as-deposited and heat-treated AlCO3; however, the energy intercept for heat-treated SSCO6 is similar to that for heat-treated AlCO2. Thus the behaviour of k is probably due primarily to Maxwell Garnett absorption as discussed for AlCO2 (Section 3.1.2). The significant increase in the value of k for SSCO6 during heat treatment is associated with the decreased resistivity of metal carbide particles in the oxygenated carbon matrix, which results from changes in metal–carbon bonding states as discussed above. (The resistivity of SSCO6 decreases to less than 2 Ω m during heat treatment (see Table VI).)

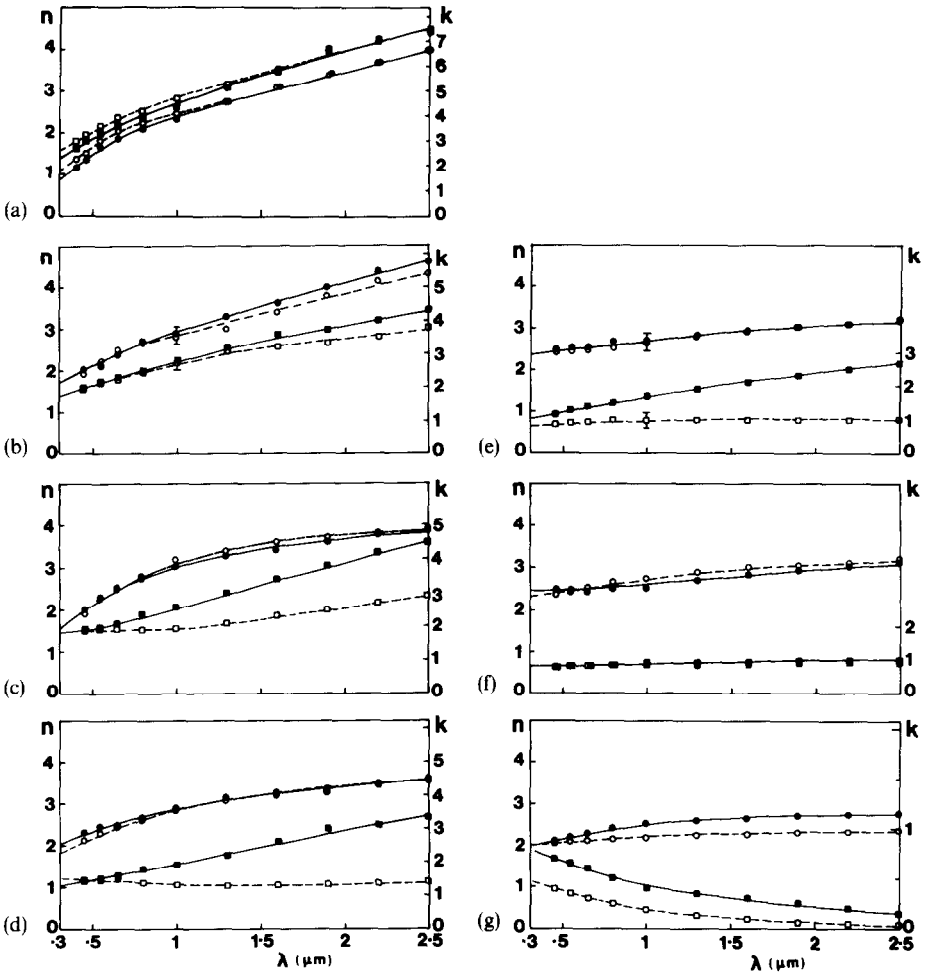

Fig. 10. Refractive index n (○, ●) and extinction coefficient k (□, ■) *vs.* wavelength λ for the homogeneous stainless steel–carbon–oxygen films ((a) stainless steel; (b) SSCO1; (c) SSCO2; (d) SSCO3; (e) SSCO4; (f) SSCO5; (g) SSCO6) described in Table VI: ○, □, as-deposited films; ●, ■, heat-treated films (1 h at 500 °C).

Both two-layer[30] and continuously graded[45] stainless steel–carbon–oxygen materials have been used to fabricate the absorbing layers of selective surfaces. The material SSCO6 with $n > 2.0$ and $k \approx 0.5$ at 0.5 μm (k increasing to about 0.7 after heat treatment) is not ideally suited as an antireflection layer; consequently solar absorptances of 0.89 or less were obtained for these selective surfaces. The application of a superior antireflection layer such as Al_2O_3 is required to produce high (greater than 0.92) values of absorptance[30].

3.4.4. O_2 reactive gas

The properties of four stainless steel–oxygen composite materials (SSO1–SSO4) are summarized in Table VI and Fig. 11. Only the composition of SSO3 changes significantly during heat treatment because of oxygen loss from the

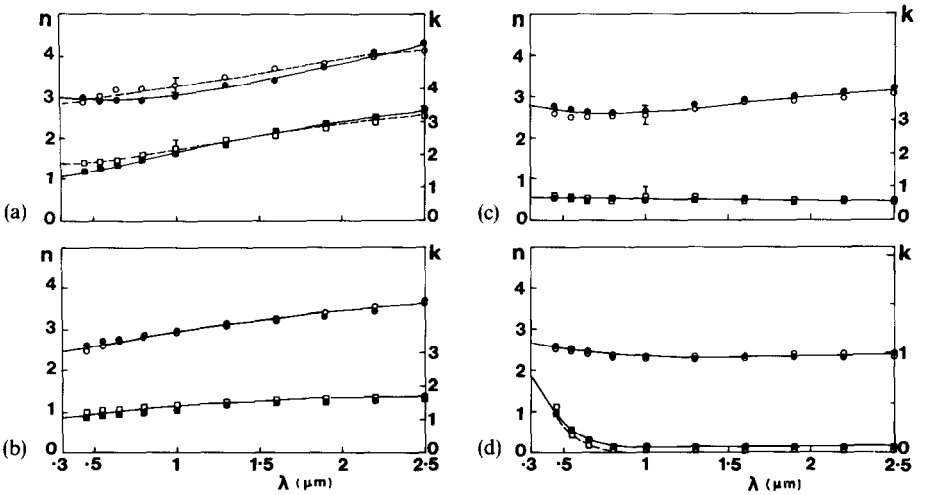

Fig. 11. Refractive index n (○, ●) and extinction coefficient k (□, ■) *vs.* wavelength λ for the homogeneous stainless steel–oxygen films ((a) SSO1; (b) SSO2; (c) SSO3; (d) SSO4) described in Table VI: ○, □, as-deposited films; ●, ■, heat-treated films (1 h at 500 °C).

film. The metal:oxygen atomic ratio in SSO4 is close to 2:3 indicating that this material consists predominantly of the oxides Fe_2O_3 and Cr_2O_3.

The deposition rates for SSO1–SSO3 are high in comparison with those of all other materials investigated in this work; however, an extremely low rate is obtained for the dielectric material SSO4. A continuous range of optical properties may be produced without difficulty, and heat treatment at 500 °C had negligible effect on the optical constants. Almost identical n and k values have been measured by Thornton[30] for an as-deposited material produced under similar conditions to those for SSO4. The strong dependence of the extinction coefficient of SSO4 on wavelength is indicative of an energy gap. Analysis similar to that illustrated in Fig. 5 gave the values of E_g listed in Table III. The energy gap decreases during heat treatment causing a small increase in k.

Although stainless steel–oxygen materials may be continuously graded, the dielectric material SSO4 with $n > 2.5$ is unsuitable as an antireflection layer. Selective surfaces incorporating single layers and two layers of stainless steel–oxygen materials have been produced, but application of an Al_2O_3 film as an antireflection layer was necessary to obtain solar absorptances above 0.9 [30].

3.5. Titanium cathode

3.5.1. CO reactive gas

The properties of three Ti–C–O composite materials, TiCO1–TiCO3, are summarized in Table VII and Fig. 12. Only the composition of TiCO3 changes significantly during heat treatment with a loss of oxygen from the material. This is probably associated with the large thickness decrease for TiCO3 films. The material TiCO3, containing only about 5 at.% metal, is very similar to AlCO3 (see Section 3.1.2). A considerable decrease in deposition rate occurs from material TiCO2 to TiCO3 because of the transition from the metal mode to the dielectric mode. A continuous range of optical properties may be produced for this material, but

TABLE VII

DEPOSITION PARAMETERS AND FILM PROPERTIES FOR MATERIALS PRODUCED BY REACTIVE SPUTTERING OF A TITANIUM CATHODE (SEE TABLE I FOOTNOTE FOR DETAILS)

Specimen	*Sputtering system*	*Argon pressure* (Pa)	*Reactive gas flow* (arbitrary units)	*Deposition rate* ($nm\ s^{-1}\ kW^{-1}$)	*Relative deposition rate*	*Film status*	*Film thickness* (nm)	*Resistivity* ρ (Ω m)	*Composition of thick (greater than 0.4 μm) films* (at.%)			
									Ti	*C*	*O*	*N*
TiCO1	CM1	0.4	0.83	0.78	0.53	AD	21	7×10^{-6}	46	42	10	
						HT500	20	1×10^{-5}	46	42	10	
TiCO2	CM1	0.4	0.95	0.52	0.35	AD	15	0.01	42	47	10	
						HT500	14	> 2.0	40	48	11	
TiCO3	CM1	0 ($P_{CO} = 0.4$)	1.0	0.13	0.10	AD	88	> 2.0	5	65	30	
						HT500	72	0.4	5	74	21	
TiO1	CM1	0.4	0.1	0.63	0.43	AD	36	5×10^{-6}	82		18	
						HT500	38	5×10^{-6}	76		22	
TiO2	CM1	0.4	1.0	0.05	0.03	AD	125	> 2.0	31		69	
						HT500	110	> 2.0	32		67	
TiN1	CM1	0.4	0.1	0.50	0.34	AD	14	5×10^{-6}	65		8	25
						HT500	13	9×10^{-6}	58		16	24
TiN2	CM1	0 ($P_{N_2} = 0.4$)	1.0	0.23	0.16	AD	14	2×10^{-4}	38		14	47
						HT500	14	1×10^{-4}	38		14	47
TiN3	CM1	0 ($P_{N_2} = 1.5$)	1.0	0.28	0.19	AD	22	4×10^{-3}	35		14	50
TiN4	CM1	0 ($P_{N_2} = 3.0$)	1.0	0.15	0.11	AD	40	> 2.0				

optical properties change rapidly over a narrow range of reactive gas flows near the transition. The optical properties of TiCO1–TiCO3 are similar to those of AlCO1–AlCO3. Heat treatment results in decreases in k for TiCO1 and TiCO2 because of oxidation of metal carbide or metal particles in the films. The extinction coefficient of as-deposited and heat-treated TiCO3 indicates the existence of an energy gap. Analysis similar to that illustrated in Fig. 5 produced the values for the energy intercept E_g listed in Table III. The values of E_g for as-deposited and heat-treated films of TiCO3 are almost identical with those for AlCO3, because of the similarity in compositions. However, the low value of the resistivity (and high value of k) for heat-treated TiCO3 (Table VII) suggests that Maxwell Garnett absorption associated with titanium carbide or titanium impurity in the oxygenated carbon is significant. Because of the low value of its electrical resistivity, TiCO3 has a higher k value than AlCO3 after heat treatment. In addition, the more rapid change in optical properties with reactive gas flow rate (or partial pressure) renders the Ti–C–O materials less suitable than Al–C–O materials for graded selective surfaces because larger tolerances are acceptable in the control of sputtering parameters for the latter materials.

3.5.2. O_2 reactive gas

Reactively evaporated Ti–O composite materials have been investigated as antireflection coatings on titanium metal for selective solar absorbers[46]. The reactive evaporation process allowed production of TiO_x with x varying from 1.8 to 2.0, with associated changes in the values of n and k. Similar selective surfaces have also been produced by the thermal oxidation of titanium in air[47,48]. Titanium oxide (TiO_2) films produced by evaporation[49] and sputtering[4,16,32,50–52] have been studied as a high refractive index material for optical filters and solar control films.

Similarly to Al–O and Cr–O composite materials, the optical properties of Ti–O materials were found to change rapidly over a narrow range of reactive gas flows (or partial pressures). Consequently the deposition of Ti–O materials with a continuous range of optical properties was not achieved. Deposition of materials with a continuous range of optical properties has been achieved by Schiller *et al.*[50] by operating a d.c. magnetron–plasmatron (target diameter, 130 mm) over a narrow range of partial pressures of O_2. The control of the properties of films sputtered from an extended post cathode is apparently more difficult because of the small variations in reactive gas concentration and sputter rate along the length of the cathode. The properties of two Ti–O composite materials TiO1 and TiO2, typical of the metal mode and dielectric mode respectively, are summarized in Table VII and Fig. 13. An extremely large difference in deposition rate for the two materials results from the transition from the metal mode to the dielectric mode. The composition of the as-deposited material TiO2 is close to that of TiO_2 with about 10% oxygen excess. The refractive index of TiO2 ($n \approx 2.3$ at 0.5 μm) is 5%–10% lower than observed in other work[51,52]. This may be a consequence of enhanced film porosity caused by the higher sputter gas pressure in our experiments and the oxygen excess in the material. For wavelengths greater than 0.4 μm, $k = 0$ because of an energy band gap of about 4 eV in TiO_2 [52]. The particularly large thickness change for TiO2 during heat treatment is probably associated with an increase in packing density and, as suggested by the compositional results (Table VII), a loss of about half the excess oxygen in the film.

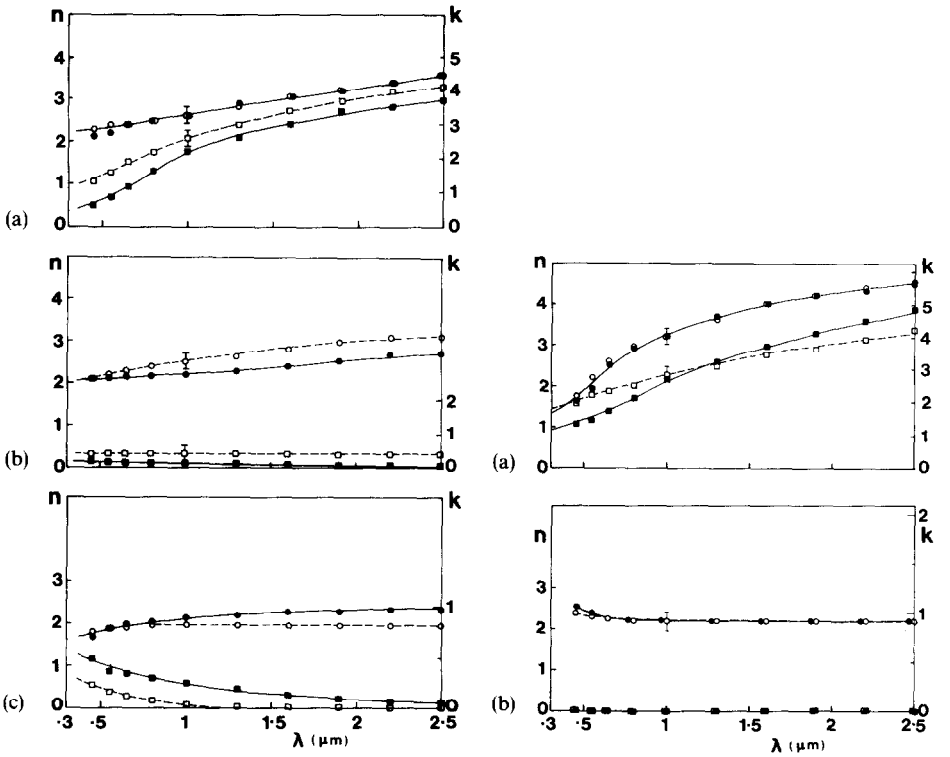

Fig. 12. Refractive index n (○, ●) and extinction coefficient k (□, ■) *vs.* wavelength λ for the homogeneous Ti–C–O films ((a) TiCO1; (b) TiCO2; (c) TiCO3) described in Table VII: ○, □, as-deposited films; ●, ■, heat-treated films (1 h at 500 °C).

Fig. 13. Refractive index n (○, ●) and extinction coefficient k (□, ■) *vs.* wavelength λ for the homogeneous Ti–O films ((a) TiO1; (b) TiO2) described in Table VII: ○, □, as-deposited films; ●, ■, heat-treated films (1 h at 500 °C).

The relatively high n value of TiO2, and the difficulty involved in obtaining a continuous gradation in optical properties, renders sputtered Ti–O materials unsuitable for graded selective absorbing surfaces.

3.5.3. N_2 reactive gas

Reactively evaporated, reactively sputtered and chemically vapour-deposited Ti–N materials have been developed for several applications. Titanium nitride films (usually of composition close to TiN) have been intensively studied for decorative coatings[3] and hard coatings[2]. The intrinsic solar selectivity of Ti–N composite materials associated with their high electrical conductivity has also led to their investigation for bulk selective solar absorbers[53–57]. Selective absorbing surfaces consisting of a single homogeneous thin film of substoichiometric TiN_x deposited onto a low emittance metal have also been produced[58].

The properties of two Ti–N composite materials TiN1 and TiN2 are summarized in Table VII and Fig. 14. Both materials contain a significant proportion of oxygen because of the high reactivity of titanium with residual water vapour in the sputtering chamber. Although the material TiN2, which is sputtered in pure N_2 gas, has low resistivity and so cannot be classified as a dielectric material,

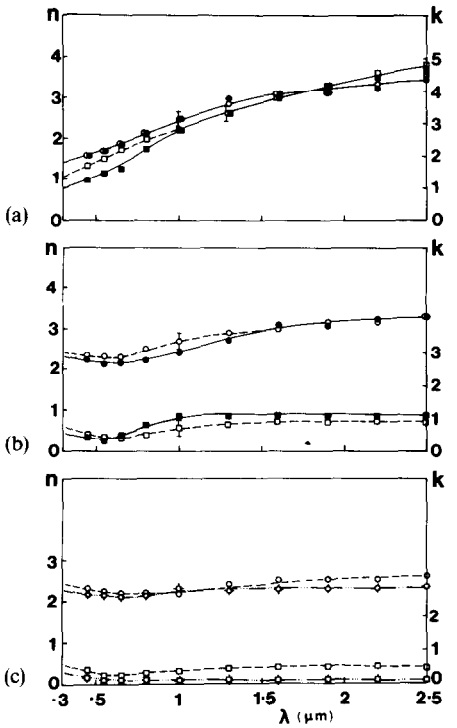

Fig. 14. Refractive index n (○, ●, -◇-) and extinction coefficient k (□, ■, -□-) *vs.* wavelength λ for the homogeneous Ti–N films ((a) TiN1; (b) TiN2; (c) TiN3 (○, □) and TiN4 (-◇-, -□-)) described in Table VII: ○, □, as-deposited films; ●, ■, heat-treated films (1 h at 500 °C).

the deposition rate of TiN2 is less than half that of TiN1, indicating that a weak transition from the metal mode to the dielectric mode occurs. The material TiN2 contains a large excess of nitrogen compared with the stoichiometry of TiN. Assuming that oxygen is bonded in the film in the form of TiO_2, the material TiN2 contains titanium and nitrogen bonded in the ratio 2:3. Optical properties similar to those of TiN2 have been obtained by Martin *et al.*[56] for a reactively ion-beam-sputtered Ti–N composite.

The relatively high values of n and k for TiN2 render it unsuitable as an antireflection layer for the graded absorbing layer of a selective surface. However, recent work on the effect of sputter gas pressure on the optical properties of reactively sputtered composite materials[31] indicated that both n and k can be reduced by development of structure and voiding in films sputtered in high gas pressures. In particular, significant (perhaps tenfold) reductions in k can occur, as a consequence of significant increases in film resistivity. The properties of two as-deposited Ti–N composite materials TiN3 and TiN4, sputtered in N_2 (no argon) at pressures of 1.5 Pa and 3 Pa respectively, are summarized in Table VII and Fig. 14. The composition of TiN3 is similar to that of TiN2 (in particular the oxygen content has not increased); however, the value of n has been reduced by about 20% for IR wavelengths while that of k has been reduced by about 50% for the full solar spectrum. Doubling the N_2 sputter gas pressure to 3 Pa results in a marginal

decrease in the value of n but a further twofold to fivefold decrease in k. The resistivities of TiN3 and TiN4 have also increased correspondingly. The material TiN4 is more suitable as an antireflection layer; however, sputtering in high gas pressures invariably leads to a decrease in sputtering rate (see Table VII).

4. CONCLUSIONS

Sputtering parameters, compositions, optical and electrical properties and stability have been surveyed for a range of d.c. post cathode magnetron reactively sputtered materials. Several new composite materials have been identified as potentially suitable for fabrication of the absorbing layer of graded solar-selective absorbing surfaces and merit further study. These include Al–C–F (aluminium cathode, CF_4 gas), Al–C–O (aluminium cathode, CO gas) and Al–N (aluminium cathode, N_2 gas). An important advantage of the aluminium cathode for preparation of the graded absorbing layer is that the same aluminium cathode may be sputtered (in pure argon) to fabricate a low emittance metal base layer for the selective surface, thus offering the possibility of an extremely simple mass production system containing only one cathode[28,59]. The detailed optical constants measured for these materials allow theoretical optimization of selective absorbing surfaces by the construction of multilayer stack models. Theoretical and experimental work on such selective surfaces will be reported elsewhere[60].

Other materials such as stainless steel–carbon–oxygen (stainless steel cathode, CO gas) and stainless steel–oxygen (stainless steel cathode, O_2 gas) composites may be continuously graded without difficulty but require an additional material of low n value (less than 2.0) and low k value (approximately zero) to be applied as an antireflection coating to achieve acceptable solar absorptances. The detailed optical constants determined here should allow modelling of selective surfaces with various antireflection coatings. Materials incorporating titanium are less suitable for graded selective surfaces.

Materials with suitable properties as antireflection coatings include the well-known materials Al–O (aluminium cathode, O_2 gas), Si–N (silicon cathode, N_2 gas), Si–O (silicon cathode, O_2 gas) and the newly identified material Al–C–F (aluminium cathode, CF_4 gas). Unfortunately Al–O produced by d.c. reactive sputtering has an extremely low deposition rate, while Si–N and Si–O require construction of a semiconducting silicon cathode. Although the properties of Al–C–F show some deterioration at temperatures above 200 °C, this material has the advantage of a high rate of deposition with extremely low n and k values. This material in particular merits further detailed study for possible application as an antireflection layer or as the low refractive index component in multilayer stacks. A study of this and similar materials produced in a d.c. planar magnetron is at present in progress.

ACKNOWLEDGMENTS

The authors would like to thank Dr. S. Craig and S. P. Chow for useful discussions, Chou Bangwei for evaporation of the Cr–O samples, Professor N. Hush of the School of Chemistry, University of Sydney, for the use of spectrophotometric facilities and D. Benson for microprobe analyses. We acknowledge the assistance of

P. Kerdraon in maintaining the coating system CM3. This research was supported by the New South Wales State Government and by His Royal Highness Prince Nawaf Bin Abdul Aziz of the Kingdom of Saudi Arabia through the Science Foundation for Physics within the University of Sydney.

REFERENCES

1 J. L. Vossen and W. Kern (eds.), *Thin Film Processes*, Academic Press, New York, 1978, pp. 75, 131.
2 W. D. Munz, D. Hofmann and K. Hartig, *Thin Solid Films, 96* (1982) 79.
3 A. Mumtaz and W. H. Class, *J. Vac. Sci. Technol., 20* (1981) 345.
4 W. D. Munz, S. R. Reineck and G. Kienel, *Proc. 7th Int. Conf. on Vacuum Metallurgy, Tokyo, Japan, November 26–30, 1982*, Iron and Steel Institute of Japan, Tokyo, 1982, p. 641.
5 J. A. Thornton, *Proc. of the American Electroplaters' Society on Coatings for Solar Collectors Symp., Atlanta, GA, 1976*, in *Plat. Surf. Finish.*, (October 1980) 46.
6 J. A. Thornton, D. G. Cornog, R. B. Hall and L. C. DiNetta, *J. Vac. Sci. Technol., 20* (1982) 296.
7 E. V. Gerova, N. A. Ivanov and K. I. Kirov, *Thin Solid Films, 81* (1981) 201.
8 I. T. Ritchie and B. Window, *Appl. Opt., 16* (1977) 1438.
9 S. Craig and G. L. Harding, *Thin Solid Films, 101* (1983) 97.
10 G. L. Harding and T. T. Moon, *Sol. Energy Mater., 7* (1982) 113.
11 G. L. Harding, B. Window, D. R. McKenzie, A. R. Collins and C. M. Horwitz, *J. Vac. Sci. Technol., 16* (1979) 2105.
12 L. N. Hadley, Transmittance and reflectance *vs.* thickness/wavelength for thin films, available from L. N. Hadley, Colorado State University, CO, U.S.A.
13 L. N. Hadley and D. M. Dennison, *J. Opt. Soc. Am., 37* (1947) 451.
14 I. T. Ritchie and G. L. Harding, *Thin Solid Films, 57* (1979) 315.
15 J. A. Thornton, *J. Vac. Sci. Technol., 11* (1974) 666.
16 W. J. Coleman, *Appl. Opt., 13* (1974) 946.
17 S. P. Chow and G. L. Harding, *Sol. Energy Mater.*, to be published.
18 M. Sikkens, *Sol. Energy Mater., 6* (1982) 403, 415.
19 S. Craig and G. L. Harding, *Surf. Sci., 124* (1983) 591.
20 L. Ramqvist, *J. Appl. Phys., 42* (1971) 2113.
21 O. S. Heavens, *Optical Properties of Thin Solid Films*, Butterworths, London, 1955, p. 213.
22 B. Meyerson and F. W. Smith, *J. Non-Cryst. Solids, 35–36* (1980) 435.
23 W. Paul and D. A. Anderson, *Sol. Energy Mater., 5* (1981) 229.
24 J. Tauc, R. Grigorovic and A. Vancu, *Phys. Status Solidi, 15* (1966) 627.
25 S. Craig and G. L. Harding, *Thin Solid Films, 97* (1982) 345.
26 J. Duchene, *Thin Solid Films, 8* (1971) 69.
27 H. Yamashita, K. Fukai, S. Misawa and S. Yoshida, *J. Appl. Phys., 50* (1979) 896.
28 Yin Zhiqiang, G. L. Harding, Chou Bangwei, Shi Yueyan, S. Craig, S. P. Chow, Wei Zhiyuan, Lin Ziwei and Lu Jinwen, in *Proc. International Solar Energy Society Congr., Perth, August 1983*, to be published.
29 W. D. Westwood, R. J. Boynton and S. J. Ingrey, *J. Vac. Sci. Technol., 11* (1974) 381.
30 J. A. Thornton, Development of selective surfaces, *Semi-annu. Tech. Prog. Rep.*, June 1979 (U.S. Department of Energy Contract DE-AC04-78CS35306).
31 S. Craig and G. L. Harding, *Appl. Opt., 22* (1983) 583.
32 W. D. Munz, J. Heimbach and S. R. Reineck, *Thin Solid Films, 86* (1981) 175.
33 H. G. Craighead, R. Bartynski, R. A. Buhrman, L. Wojcik and A. J. Sievers, *Sol. Energy Mater., 1* (1979) 105.
34 J. A. Thornton and J. L. Lamb, *Thin Solid Films, 96* (1982) 175.
35 G. A. Niklasson and C. G. Granqvist, *Sol. Energy Mater., 7* (1983) 501.
36 J. A. Thornton, J. L. Lamb and A. S. Penfold, Development of selective surfaces, *Final Rep.*, August 1980, p. 5 (U.S. Department of Energy Contract DE-AC04-78CS35306).
37 J. C. C. Fan and S. A. Spura, *Appl. Phys. Lett., 30* (1977) 511.
38 G. E. Carver, H. S. Gurev and B. O Seraphin, *J. Electrochem. Soc., 125* (1978) 1138.
39 G. Hass, H. H. Schroeder and A. F. Turner, *J. Opt. Soc. Am., 46* (1956) 31.

40 M. M. Koltun, *Geliotekhnika*, *6* (1970) 33 (*Appl. Sol. Energy*, *6* (1970) 65).
41 D. R. McKenzie, *Thin Solid Films*, *62* (1979) 317.
42 E. Randich and D. D. Allred, *Thin Solid Films*, *83* (1981) 393.
43 G. J. Kominiak, *J. Electrochem. Soc.*, *122* (1975) 1271.
44 L. M. Briggs, D. R. McKenzie and R. C. McPhedran, *Sol. Energy Mater.*, *6* (1982) 455.
45 G. L. Harding and B. Window, *J. Phys. (Paris), Colloq. C1*, *42* (1981) 173.
46 S. Yoshida, *Thin Solid Films*, *56* (1979) 321.
47 D. K. Edwards, J. T. Gier, K. E. Nelson and R. D. Roddick, *Sol. Energy*, *6* (1962) 1.
48 D. L. Douglass and R. B. Pettit, *Sol. Energy Mater.*, *4* (1981) 383.
49 H. K. Pulker, G. Pasold and E. Ritter, *Appl. Opt.*, *15* (1976) 2986.
50 S. Schiller, G. Beister, S. Schneider and W. Sieber, *Thin Solid Films*, *72* (1980) 475.
51 S. Schiller, G. Beister, W. Sieber, G. Schirmer and E. Hacker, *Thin Solid Films*, *83* (1981) 239.
52 K. G. Geraghty and L. F. Donaghey, *Thin Solid Films*, *40* (1977) 375.
53 B. O. Seraphin, in B. O. Seraphin (ed.), *Optical Properties of Solids: New Developments*, North-Holland, Amsterdam, 1976, p. 927.
54 J. Rivory, J. M. Behaghel, S. Berthier and J. Lafait, *Thin Solid Films*, *78* (1981) 161.
55 L. Roux, J. Hanus, J. C. Francois and M. Sigrist, *Sol. Energy Mater.*, *7* (1982) 299.
56 P. J. Martin, R. P. Netterfield and W. G. Sainty, *Vacuum*, *32* (1982) 359.
57 B. Karlsson, R. P. Shimshock, B. O. Seraphin and J. C. Haygarth, *Sol. Energy Mater.*, *7* (1983) 401.
58 R. Blickensderfer, D. K. Deardorff and R. L. Lincoln, *Sol. Energy*, *19* (1977) 429.
59 G. L. Harding, *Sol. Energy Mater.*, *7* (1982) 123.
60 G. L. Harding, Yin Zhiqiang, S. Craig and S. P. Chow, *Sol. Energy Mater.*, *10* (1984) 187.